Biophysical Journal, Volume 99

Supporting Material

Title: Fetuin-A is a Mineral Carrier Protein: Small Angle Neutron Scattering

Authors: Alexander Heiss, Vitaliy Pipich, Willi Jahnen-Dechent, and Dietmar Schwahn

Sample Parameters and Scattering Length Density of Fetuin-A

The relevant physical properties, i.e. mass density d, molar weight M, molar volume V, chemical formula, and coherent scattering length density ρ, of all sample components are summarized in Table S1. Regarding the mineral phase the two polymorphs hydroxyapatite (HAP) and octacalcium phosphate (OCP) have been taken into consideration. The coherent scattering length density ρ is a measure of the interaction between neutrons and sample. The value for water is known whereas the ones for HAP and OCP were calculated on the basis of the chemical formula and the corresponding molar volume V of the unit cell (9). Mass density and molar weight of BF were assessed by ultracentrifugation.

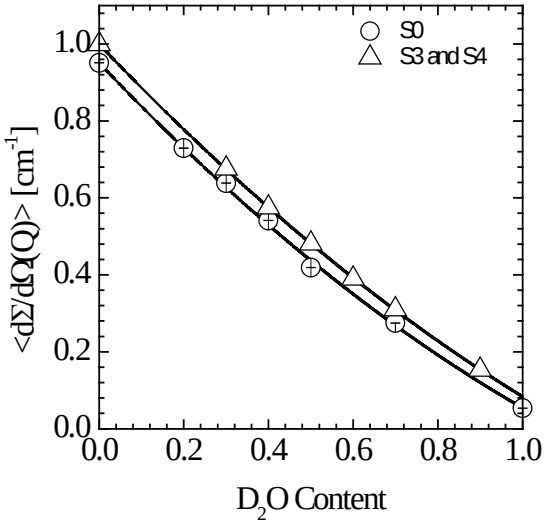

FIGURE S1. Scattering of buffer (S0) and of BF controlled mineralization (S3, S4) over a range of D_2O concentrations (Table 1). On average the background scattering of the mineralization is increased by 4.3×10^{-2} cm^{-1}.

Fig. S1 depicts the averaged scattering of the buffer (S0) as well as the large Q intensity of the BF controlled mineralized samples (S3, S4) along a H_2O/D_2O gradient which is mainly due to incoherent and thermally diffuse scattering. A pronounced decrease in scattering intensity from 0.95 to 0.054 cm^{-1} with increasing D_2O content was observed. As the protein scattering (samples

S2-4) is only between 1 - 10 % of the solvent scattering, proper background correction is essential to ensure a high accuracy of the data.

The scattering length density of BF in buffer (Tab. S1, sample S1) was collected in parallel to all other samples in order to improve precision and reliability. In Fig. 3A the scattering patterns of S1 and S2 in H_2O are depicted in absolute units. The extrapolated scattering at Q=0 was determined from a fit (depicted as solid line) of Guinier's law (Eq 3) additionally delivering the radius of gyration. In Fig. 3B the scattered intensity at Q=0 is plotted versus the D_2O content. A fit of the data with a parabola gives a minimum at Φ_{D2O} = 0.448±0.001, which is within a reasonable range for proteins (23). As ρ of the solvent as well as of the protein depends linearly on the D_2O content, it follows for the scattering contrast $\Delta\rho^2 = (\rho_{BF} - \rho_W)^2 \propto \Phi^2$ and thus validating according to Eq. 2 the parabolic fit of $d\Sigma/d\Omega(0)$.

The known BF concentration Φ and its volume V allow the determination of the coherent scattering length density (Fig. 2) according to the relationship in Table S1 which was derived from fitting the experimental data.

	d [g/ml]	M [kDa]	V [10^{-22}cm^3]	Chemical Formula	ρ [10^{10} cm^{-2}]
Water	**1**	**---**		**D_2O [Φ] + H_2O[1-Φ]**	**-0.561+6.951 Φ**
BF	**1.317**	**52.8**	**665.7**	**---**	$(2.48 \pm 0.01) + (0.12 \pm 0.02)\,\Phi$
Calcium	**1.55**	**0.04008**	**0.429**	**Ca**	**1.096**
Chloride	**3.215**	**0.03545**	**0.183**	**Cl**	**5.233**
Calcium Phosphate	**3.09**	**0.971**	**5.218**	**$Ca_{10}(PO_4)_6$**	**4.17**
Posner Cluster	**5.08 (4.55)**	**0.931**	**3.04 (3.4±.0.2)**	**$Ca_9(PO_4)_6$**	**6.99 (6.3±0.3)**
HAP	**3.2**	**1.004**	**5.21**	**$Ca_{10}(PO_4)_6(OH)_2$**	**4.26+0.4 Φ**
OCP	**2.61**	**0.983**	**6.25**	**$Ca_8H_2(PO_4)_6$ 5(H_2O)**	**3.07+1.99 Φ**

Table S1: Parameters of relevant sample components. Φ represents the D_2O volume fraction, M_W molar weight, and d the mass density. The Posner cluster parameters in the brackets were determined from SANS.

Colloidal Calcium Phosphate - Fetuin-A Composites

We performed measurement at smaller Q in order to assess the scattering of the larger CPPs. As the KWS2 instrument newly set up at the FRM II (Garching, Germany) was limited to a maximum sample-to-detector distance of 8 m, we had to adjust the neutron wavelength to 19 Å in

order to reach a minimum Q of about $4x10^{-3}$ $Å^{-1}$. Fig. S2A depicts the scattering patterns of secondary CPPs in sample S3 at different contrasts. The lowest scattering was detected at 60 % D_2O. CPP scattering patterns were analyzed according to Eq. 6 taking incoherent scattering as

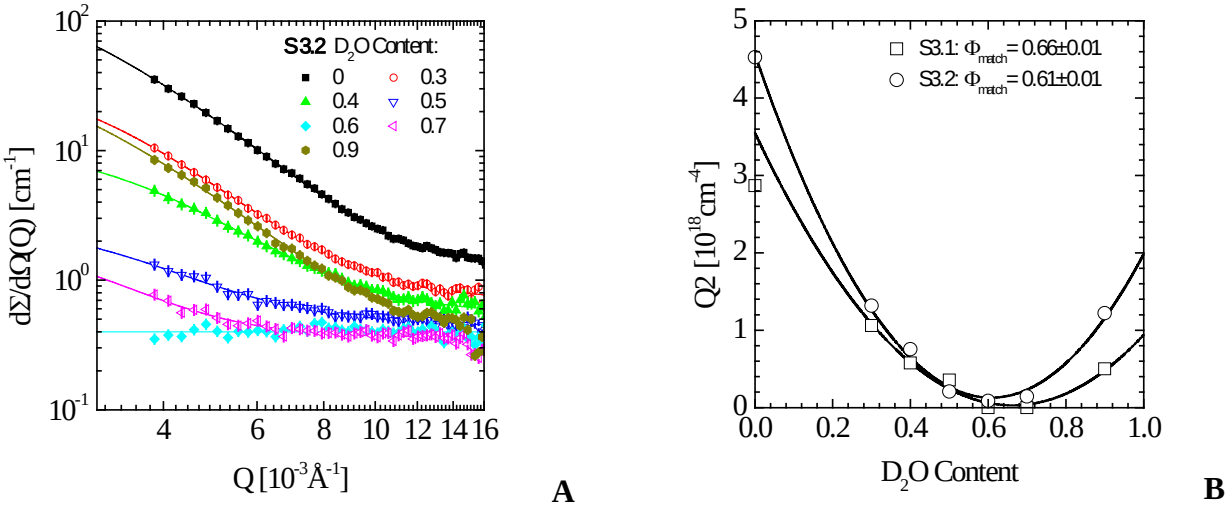

FIGURE S2. A. Scattering patterns of CPPs in S3 at different contrast conditions. A wavelength of 19 Å and a sample-to-detector distance of 8 m had to be adjusted for these measurements. The patterns were fitted according to Eq. 5 (solid lines). The intensity of the secondary CPPs showed a minimum at 60 % D_2O. **B**. Second moment Q2 (Eq. 6) derived from the fitted curves of Fig. S2 A. The minima of Q2 for primary and secondary CPPs were located between 60 and 70 % D_2O confirming previous studies.

Sample	**S3.1**	**S3.2**	**S4.1**	**S4.2**
Φ_{D2O}	0.66±0.01	0.61±0.01	0.72±0.02	0.66±0.02
ρ_{CPP} [$10^{10}cm^{-2}$]	4.03±0.1	3.68±0.1	4.44±0.2	4.03±0.2
ρ_{BF} [$10^{10}cm^{-2}$]	2.55±0.07	2.54±0.07	2.56±0.07	2.55±0.07
ρ_{OCP} [$10^{10}cm^{-2}$]	4.38±0.02	4.28±0.02	4.50±0.04	4.38±0.04
C_{BF}	0.20±0.01	0.35±0.02	0.03±0.004	0.19±0.02
φ_{Min} := Φ_{Min}(CPP)/Φ_{Min}(initial weight)	0.47±0.03 (0.44±0.02)	0.70±0.06 (0.59±0.03)	0.45±0.06 (0.32±0.02)	0.45±0.06 (0.29±0.02)
φ_{BF} [10^{-2}]:= Φ_{BF}(CPP)/Φ_{BF}(initial weight)	1.6±0.2	4.2±0.5	1.1±0.2	7.5±1.3

TABLE S2. CPP parameters derived from SANS. The values in brackets in row 6 refer to another unpublished CPP-SANS investigation by A. Heiss, V. Pipich, W. Jahnen-Dechent and D. Schwahn.

well as scattering arising from CPMs, e.g. $d\Sigma / d\Omega(0)$ as constant. Their second moment Q2 was determined relying on the fits (Eq. 6) depicted as solid lines. Q2 plotted in Fig. S2B proved to be the most reliable parameter regarding a correct assessment of the mean scattering length density of the CPPs. The Q2 minima are located between 60 and 70 % D_2O, which is in fair agreement with our earlier studies (9).

Table S2 compiles the CPP parameters. Row one shows the D_2O volume fractions Φ_{D2O} in the aqueous solvent matching the mean coherent scattering length density ρ of the CPPs (Fig. S2). The BF volume fraction C_{BF} inside the CPPs was derived from the scattering length densities ρ of the CPPs, BF, and OCP (rows 2-4). Previous studies suggested that the mineral polymorph in the CPPs is OCP (9). Its mineral volume fraction was derived from $(1\text{-}C_{BF})$. Row six lists the fractions of mineral enclosed in the CPPs φ_{Min} which were derived from the second moment Q2 (Fig. S2 B) and the corresponding scattering length density ρ_{CPP}.

Although the SANS setup was optimized to detect the scattering of the BF molecules in the high Q range, thus limiting the Q regime of our SANS diffractometer, we retrieved a CPP data set at the lower limit of the Q range. The resulting CPP parameters compared well with published CPP structure determinations in the low Q range (Table S2: Values in brackets of row six), which is consequently inherently more precise at the CPP scale (9,10). The validity of our approach was also confirmed by a comparison of the non-CPP mineral fraction $(1\text{-}\varphi_{Min})$ with the chemical "free" Ca^{2+} ion analysis (Table 2). Both techniques yielded consistent results with the exception of sample S4.2 where a non-CPP mineral fraction of about 89% (Table 3) and 71% ($1\text{-}\varphi_{Min}$ derived from φ_{Min}=0.29, Table S2), respectively, was detected by SANS compared to 32% (Table

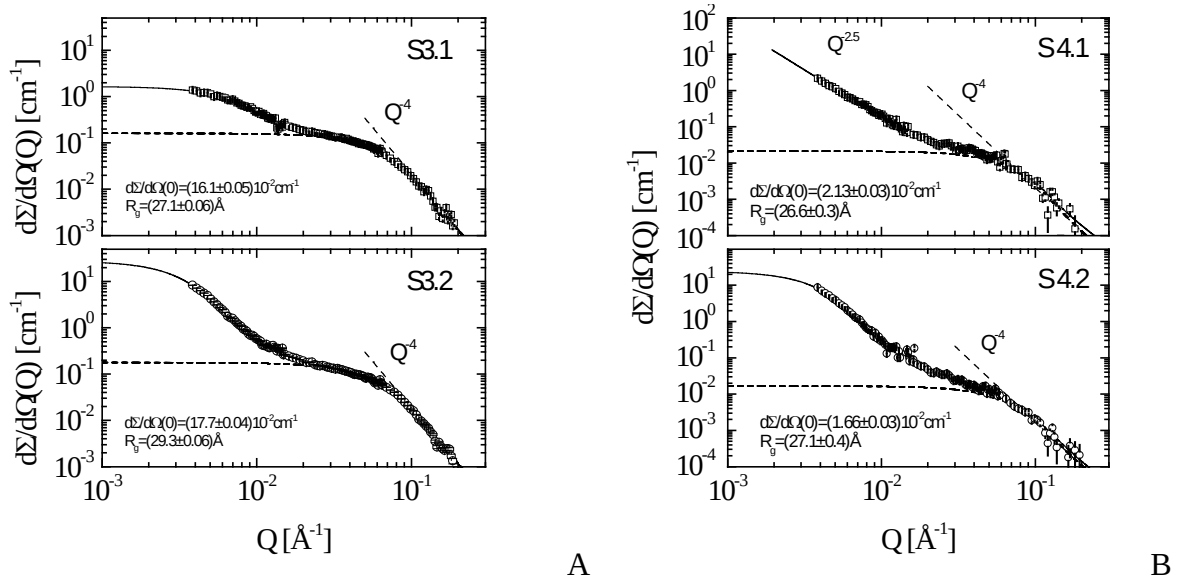

FIGURE S3 A, B. Scattering cross-section of samples S3 and S4 in 90 % D_2O in the presence of primary or secondary CPPs. The dashed lines represent a fit of the CPM scattering. The radii of gyration obtained by fitting according to Eq. 5 are slightly smaller than 30 Å corresponding to the size of BF.

2) by ultrafiltration. The value for φ_{Min} is probably too low, suggesting minor CPP sedimentation due to poor stability at this low BF concentration.

Scattering cross-sections of samples S3 and S4 in 90 % D_2O aqueous solution

The scattering patterns of S3 and S4 as depicted in Fig. S3A, B were measured in 90 % D_2O and analyzed quantitatively in terms of the underlying scattering laws, as these samples are characterized by a relatively large scattering contrast and a low incoherent background (Figs. 2 and S1). The corresponding scattering patterns were plotted in double logarithmic scale and were fitted according to Eq. 5 indicated by the solid and dashed lines. Monomer scattering (dashed line) became dominant at $Q > 0.03$ Å^{-1} and clearly showed the Guinier and Q^{-4} Porod power law regimes (Eqs. 3 and 4). The results of this analysis are compiled in Tables S3 and 3.

Sample	**S1**	**S2**	**S3.1**	**S3.2**	**S4.1**	**S4.2**
Φ_{D2O}	0.447±0.001	0.459±0.001	0.476±0.004	0.503±0.005	0.634±0.005	0.678±0.007
ρ_{CPM} $[10^{10}cm^{-2}]$	-	2.63±0.007	2.75±0.03	2.94±0.04	3.85±0.04	4.15±0.05
ρ_{BF} $[10^{10}cm^{-2}]$	2.53±0.01	2.54±0.01	2.54±0.01	2.54±0.01	2.56±0.02	2.56±0.02
$d\Sigma/d\Omega$ (0) $[10^{-2}$ $cm^{-1}]$	11±0.09	11.9±0.07	16.1±0.05	17.7±0.04	2.13±0.03	1.66±0.03
R_g [Å]	27.4±0.3	29.3±0.2	27.1±0.06	29.3±0.06	26.6±0.3	27.1 ±0.4
P_4 $[10^{26}cm^{-5}]$	-	-	2.14±0.6	1.87±0.02	0.207±0.01	0.17±0.01
Q2 $[10^{19}cm^{-4}]$	-	-	3.26	2.98	0.394	0.303

TABLE S3. CPM parameters in the presence of primary (SX.1) and secondary (SX.2) CPPs (X=3,4) inferred from SANS contrast variation. Scattering parameters in row 4-7 of samples S1 and S2 were determined in pure H_2O while S3 and S4 were determined in 90 % D_2O.

Computer Graphics

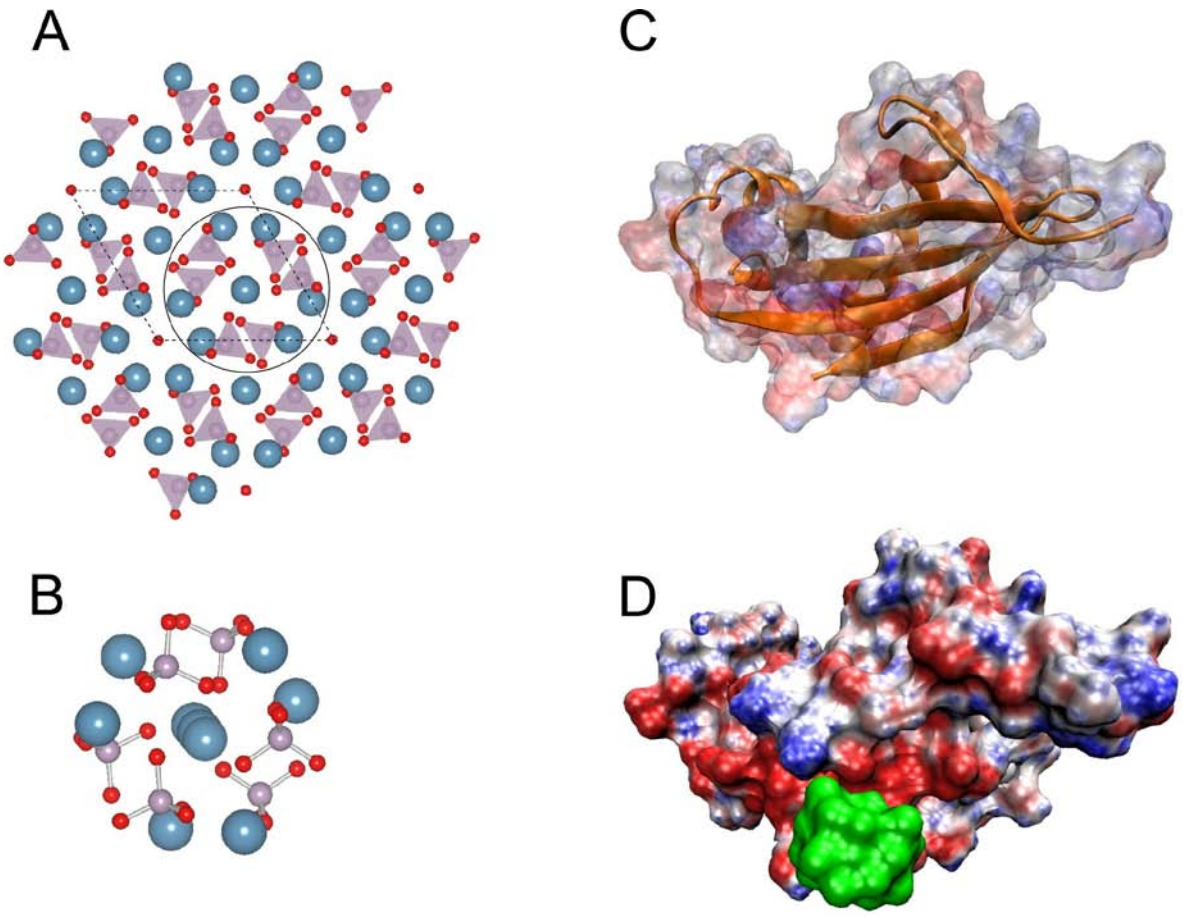

FIGURE S4. A. View of the crystal structure of hydroxyapatite along the [001] axis. The dotted lines confine the hexagonal unit cell. The circle represents a Posner cluster as a building block of the apatite structure. **B**. 3D view of a $Ca_9(PO_4)_6$ Posner cluster. **C.** View onto the acidic β-sheet of the model of the aminoterminal fetuin-A domain D1 (7). The corresponding surface is plotted semitransparent. **D**. Electrostatic surface (negative charge red, positive charge blue) plot of the protein domain with a Posner cluster (green) attached the most acidic surface area.